Characterization of Tissue Response and in Vivo Degradation of Cholecyst-Derived Extracellular Matrix

Krishna Burugapalli and Abhay Pandit*

Department of Mechanical and Biomedical Engineering, and National Centre for Biomedical Engineering Science, National University of Ireland, Galway, Ireland

Received May 21, 2007; Revised Manuscript Received August 22, 2007

A rat subcutaneous implantation model was used to evaluate the in vivo degradation and tissue response of cholecyst-derived extracellular matrix (CEM). This response was compared to that of glutaraldehyde (GA) cross-linked CEM and porcine heart valve (HV), which are designated as GAxCEM and GAxHV, respectively. Tissue composition, inflammatory cell distribution, and angiogenesis at the implant site were quantified using stereological parameters, thickness (T_a), volume fraction (V_v), surface density (S_v), length density (L_v), and radius of diffusion (R_{diff}). CEM was completely infiltrated with host tissue at 21 days and resorbed by 63 days. GAxCEM was also infiltrated with host tissue, while GAxHV matrix was impermeable to host tissue infiltration. Both GAxCEM and GAxHV retained their scaffold integrity until 63 days with no apparent degradation. A fibrous tissue of thickness <52 μm, rich in collagen and vasculature, surrounded all scaffolds, and from 21 to 63 days the fibrous tissue showed maturation with a significant increase in their fibrocyte content. No signs of acute inflammatory response were observed in the study period for any of the scaffolds, while the chronic inflammatory response was predominated with macrophages for all scaffolds except for CEM at 63 days. A higher degree of giant cell formation was observed with GA cross-linked scaffolds. From 21 to 63 days, lymphocytic response decreased for CEM, while it increased significantly for GAxHV. Angiogenesis/neo-vascularization was uniform for CEM (reaching the core), significantly lower for GAxCEM within the implant area as compared to CEM, while restricted to the exterior of GAxHV matrix. In summary, CEM was a fast degrading scaffold that induced a transitional inflammatory response accompanied by gradual resorption and replacement by host connective tissue as compared to the very slow degrading GA cross-linked controls, GAxCEM and GAxHV, which caused a sustained chronic inflammatory response and remained at the site of implantation until the end of the study period of 63 days.

Introduction

Extracellular matrix (ECM) is the non-cellular part of tissue, which has wide ranging structural and functional role in cell, tissue, and organ morphogenesis, maintenance, and host response to injury. Considerable efforts are being directed to design tissue engineered scaffolds that mimic the natural ECM.[1,2] In this direction, there has been a growing interest in decellularized xenogenic/allogenic ECM for tissue engineering applications.[3] Furthermore, decellularized ECM scaffolds have been shown to degrade within the body and promote matrix remodeling, thereby augmenting the regeneration of damaged or missing tissues.[4,5]

In our laboratory, a new decellularized ECM, named CEM, has recently been developed. CEM is derived from the perimuscular subserosal connective tissue of the cholecyst (gallbladder) wall.[6] The assessment of the native properties has established that CEM has a mesh-like architecture, nanoscale topography appropriate for cell infiltration, tissue growth, and regeneration, adequate mechanical properties, controllable degradation, and in vitro ability to support allogenic as well as xenogenic cells.[6−8] However, before this matrix can be developed for any clinical application, it is essential to evaluate its in vivo tissue response and regenerative ability.

The primary objective of this study was to establish the in vivo life and behavior of native CEM (decellularized and non-cross-linked). Rapid scaffold degradation (within 2 months of implantation) and early resolution of acute inflammatory phase (as early as 72 h) reported for similar porcine materials[4] prompted the choice of the time points 21 and 63 days for this study. By 21 days, any effects due to surgery would be completely resolved, and the 63 day time point was chosen so that information could be gained about the terminal resorption activity involving any residual native CEM implant and/or host tissue remodeling. GAxCEM was used as a very slow degrading control that retains its scaffold integrity until the end of the study period of 63 days. In addition, the current study also utilized GA cross-linked, non-decellularized porcine heart valve (HV) as a negative control, because GA cross-linking and xenogenic cellular components are implicated in calcification and graft rejection.[5] However, in this study, a GA cross-linking concentration of 0.625% was utilized instead of the traditional extensive cross-linking by GA tanning. Bigi et al. reported that a GA cross-linking concentration of $>0.5\%$ was sufficient for near 100% cross-linking of a similar material, gelatin,[9] and CEM samples cross-linked under similar conditions as reported by Bigi et al. showed that $\geq 0.052\%$ GA was sufficient to eliminate the susceptibility of CEM to in vitro collagenase degradation.[6] Hence, 0.625% GA cross-linking concentration would be enough to achieve near 100% cross-linking and our objective of GAxCEM as a very slow degrading control that would retain its structural integrity in vivo until 63 days.

Traditionally, tissue response assessments to biomaterials/tissue engineering scaffolds have been either qualitative or semiquantitative.[10−12] Application of quantitative histomorpho-

* To whom correspondence should be addressed. Fax: +353 91 563991. E-mail: abhay.pandit@nuigalway.ie.

10.1021/bm700560k CCC: $37.00
Published on Web 10/06/2007

metric methods was restricted to a few parameters like thickness of fibrous tissue or implant,[13−15] partial volumes/volume fractions,[16,17] or absolute numbers of cells per high power field.[18−21] However, comprehensive and systematic quantitative tissue response assessments are rare. A quantitative assessment is important because it provides an objective method to describe a structure, compare two structures, study structural change, and relate structure to function.[22,23] Stereology is a science based on the principles of geometry and statistics that provides simple, powerful, fast, accurate, objective, reproducible, and verifiable methods to acquire 3D quantitative information from 2D slices.[22−26] Hence, the need for a comprehensive, robust, and objective stereological approach for the quantitative evaluation of tissue response to tissue engineered scaffolds has been recently emphasized.[22] The current study utilizes quantitative stereological approaches to quantify the tissue response to tissue engineering scaffolds implanted in a subcutaneous implantation rat model. The stereological parameters, thickness measurement (T_a, arithmetic mean thickness), volume fraction (V_v, volume per unit volume), surface density (S_v, surface area per unit volume), length density (L_v, length per unit volume), and radius of diffusion (R_{diff}, radial diffusion distance between tubular structures − blood vessel), have been utilized to obtain quantitative information and compared structural and compositional changes at subcutaneous implantation sites between treatments.

Experimental Section

All reagents unless otherwise stated were purchased from Sigma Ireland Ltd., Dublin, Ireland. Fresh cholecysts and hearts of market weight farm-reared pigs (Sean Duffy Exports Ltd., Gort, Ireland) were transported to the laboratory on ice and processed within 6 h of sacrifice.

Preparation of Scaffolds for Implantation. CEM was isolated and processed according to the procedure described by Coburn et al.[7] Briefly, excess liver tissue was removed, and then the serosal mesothelium and its underlying connective tissue from the abluminal side was cut off while the gall bladder was still full. After the serosal layer was removed, the bile was drained from the gall bladder. The neck and fundus of the cholecyst were trimmed, followed by a longitudinal incision to obtain a flat sheet of tissue. The mucosa, lamina propria, and muscularis layers were peeled from the luminal side. Any residual elements on both serosal and mucosal sides were removed by mechanical delamination. The remaining CEM was then washed in five changes of 5 min each with phosphate buffer saline (PBS), pH 7.4, under constant agitation followed by five washes of 5 min each in distilled water.

Porcine hearts were dissected, and heart valves were isolated. CEM samples for cross-linking with GA (Agar Scientific Ltd., Cambridge, UK) and HV were treated with 0.625% GA (w/v) in phosphate buffered saline (PBS), pH 7.4, for 24 h. GA cross-linked CEM (GAxCEM) and HV (GAxHV) samples were washed in five changes of PBS followed by five changes of distilled water. The CEM, GAxCEM, and GAxHV samples for implantation were cut to 10×10 mm^2 specimens, sterilized with 0.15% peracetic acid solution in sterile deionized water for 5 min, washed repeatedly in sterile Hank's Balanced Salt Solution, and stored in 5% penicillin−streptomycin solution at 4 °C for 2 days prior to implantation.

Implantation in Rats. Six week old Sprague Dawley rats (Harlan UK Ltd., Oxon, UK) weighing between 150 and 200 g were housed in the experimental animal facility at the National Centre for Biomedical Engineering Science, Galway. All animal procedures had ethical approval from the Institutional Animal Ethics Committee of the National University of Ireland − Galway, and the studies were also covered under the license issued by the Department of Health and Family Welfare, Ireland. The rats were acclimatized to local environment for 1 week prior to surgery.

The rats were anaesthetized with ketamine (100 mg/kg) and xylazine (5 mg/kg), and the dorsal skin was shaved and disinfected. Along the dorsal midline, three 15 mm longitudinal incisions were made, about 30 mm apart. At each incision, two lateral subcutaneous pockets were made. In each pocket, one 10×10 mm scaffold was immobilized at the subcutaneous level using a non-degradable suture (Ethicon 4-0 Prolene, Johnson & Johnson Ireland Ltd., Dublin, Ireland) about 10 mm away from the incision. The incisions were closed using a degradable suture (Ethicon 4-0 Vicryl, Johnson & Johnson Ireland Ltd., Dublin, Ireland). Following surgery, a daily dose of 10 mg/mL of caprofen was administered subcutaneously for 4 days from the date of surgery. The rats were caged in a controlled environment of temperature range of 15−25 °C, relative humidity of 40−70%, light to dark cycles of 14:10 h, standard pellet diet, and fresh water. The implant sites were physically observed at regular intervals.

A total of eight rats were divided into two groups of four each. Each animal received six implants ($n = 2$ per scaffold per animal). The positions of the scaffolds types were randomized such that each scaffold type occurs at least once at each of the six positions on the back of the rats for each group. The two groups of animals were sacrificed at 21 and 63 days. There were eight treatments per each of CEM, GAxCEM, and GAxHV scaffolds, per time point. At the time of sacrifice, the skin along with implant, surrounding tissue, and underlying muscle were carefully dissected from the subcutaneous site and fixed in 4% neutral buffered formalin.

Histopathology. Formalin fixed tissues were dehydrated through graded ethyl alcohol solutions (50%, 75%, 95%, and 100%), cleared with xylene, and embedded in paraffin. The processing of the tissues was done in an automatic tissue processor (Leica ASP 300, Leica Microsystems, Nussloch, Germany). Five-micrometer thick paraffin sections were stained with hematoxylin and eosin (H&E), Masson's trichrome (MT), picosirus red, von Kossa, and alizarin red stains. H&E and MT stains were used to evaluate the general histomorphology and quantitative stereological analysis at the implant sites, while von Kossa and alizarin red stains were used to evaluate calcification at implant sites. Pico-sirius red staining and bifringent polarized light microscopy were used to demonstrate the distribution of collagen at the subcutaneous implant sites. The differentially stained sections were observed under light microscope and digital images captured for stereological analysis (BX51 microscope, DP-70 digital camera, simple polarizer − analyzer and 530 nm filter for bifringence, Olympus Europe, Hamburg, Germany).

Quantitative Stereological Analysis. The different stereological methods utilized for the quantification of tissue response and degradation parameters in this study were based on the practical examples reported by Garcia et al.[22] The stereological approach is based on sampling, and sampling needs to be isotropic.[22,24] Because cutaneous tissue is an anisotropic layered structure, its stratified nature required the use of vertical uniform random sampling method to obtain isotropy in the vertical sections.[24,26−28] Six fields of view per stereological parameter, a minimum of three histology sections (~100 μm apart) per treatment, and eight treatments per test scaffold per time point were used for adequate sampling.[22] The probes/test systems (counting frames, grids, etc.) and other image analysis tools provided by an image analysis software (Image Pro Plus, Media Cybernetics, UK) were used to obtain point counts for the stereological estimations. The tissue response and degradation parameters quantified in this study included thickness and composition of fibrous tissue surrounding implant, degree and quality of host tissue infiltration into implanted scaffold, scaffold degradation, nature and distribution of inflammatory cells, as well as blood vasculature at the implant site.

The details of stereological parameters and probes used in the quantification of the different tissue response and degradation parameters are presented in Table 1, while the magnifications and distribution of fields of view for each the stereological parameters are illustrated in Scheme 1. The thickness of fibrous tissue was measured on MT stained histology sections at 400× magnification on six non-overlapping

Table 1. Stereological Methods Used in This Study for the Evaluation of Tissue Response and Degradation Parameters at Subcutaneous Implantation Site

stereological parameter	tissue response parameter	probe: orientation and dimensions	equation	refs
arithmetic mean thickness (T_a)	thickness of fibrous tissue surrounding implant	orthogonal lines from intercepts on parallel lines 50 μm apart; 400× mag.	$T_a = L \times \pi/4$	22, 24
volume fraction/ density (V_v)	volume of each tissue response zone (fibrous tissue/implant area) per total volume of subcutaneous implantation site	grid; 200 × 200 μm^2 per square; 12.5× mag.	$V_v = P_P/P_T$	22−26
	volume of each tissue component (collagen/nuclei) per total volume of the tissue response zone	grid; 10 × 10 μm^2 per square; 1000× mag.		
	volume of nuclei of each cell type per total volume of all cell nuclei	grid; 10 × 10 μm^2 per square; 1000× mag.		
surface density (S_v)	surface area of blood vessels per unit volume of tissue	cycloid grid; cycloid arc height, 10 μm; 8 arcs/line; 5 lines/grid; 1000× mag.; oriented perpendicular to vertical axis of VUR section	$S_V = 2 \times I/L_T$	22−26
length density (L_v)	length of blood vessels per unit volume of tissue	cycloid grid; cycloid arc height, 10 μm; 6 arcs/line; 6 lines/grid; 1000× mag.; oriented parallel to vertical axis of VUR section	$L_v = (2 \times I/L_T)/T_S$	22, 24, 56
radius of diffusion (R_{diff})	radial diffusion distance between blood vessels	same as that for L_v measurements	$R_{diff} = 1/\sqrt{\pi \times L_v}$	22, 57

fields of view (Scheme 1A), and the arithmetic thickness (T_a) was calculated. Stereological volume fraction (V_v) estimations of collagen, cell nuclei, cell cytoplasm, and blood vessels as a function of total volume of the tissue response zone, on MT stained histology sections at 1000× magnification (Scheme 1B), were used for the evaluation of the composition of the fibrous tissue as well as the degree and quality of host tissue infiltrating into the implant matrix. For the evaluation of scaffold degradation, the V_v values of implant area and fibrous tissue as a function of volume of total subcutaneous implantation site (implant area + fibrous tissue) were determined on MT stained sections (6 sections, ~100 μm apart) at a magnification of 12.5× (Scheme 1C). Further, the nature and distribution of inflammatory cells at the implant site was evaluated using V_v estimations of the different cell nuclei as a function of total cell nuclei. The identification of cells was based on their respective morphologies in H&E stained histology sections at a magnification of 1000× (Scheme 1B). Abbreviations and morphological criteria for classification of the different cells types used in this study are summarized in Table 2. Finally, on H&E stained histology sections at a magnification of 1000× (Scheme 1B), the nature and distribution of blood vasculature (angiogenesis) at the implant site was evaluated using the following stereological parameters: surface density (S_v), length density (L_v), and radius of diffusion (R_{diff}).

Statistical Analysis. Statistical analyses were carried out using statistical software (SPSS v.14). Statistical variances between groups were determined by one-way analysis of variance (ANOVA). Tukey's honestly significant difference test was used for post hoc evaluation of differences between groups. A p value of <0.05 was considered to be statistically significant. All data represented are expressed as mean ± standard error (SE) of mean.

Results

All rats survived the surgery and the study period and had a normal post-surgery recovery. Gross morphology of the sites of implantation did not show any ulceration, pus, or discharge. At the time of sacrifice, the remains of all scaffolds, except CEM at 63 days, were observed. The site of implantation for CEM at 63 days was identified by locating the non-degradable suture that was used to immobilize the scaffold, and the implant site was extensively sectioned and stained to check for any residual implant.

Histological Structure at Subcutaneous Implantation Site. Histologically, the remains of all scaffolds except for CEM at 63 days were observed at the subcutaneous implantation site. No signs of adverse reactions like necrosis, infection, or granuloma were observed for any of the scaffolds. Alizarin red and von Kossa stained histology sections revealed that none of the implanted scaffold variants showed any signs of calcification.

As illustrated in Figure 1A−F, the implant area for all scaffolds was surrounded by host deposited fibrous tissue (FT). The FT was composed of loose connective tissue rich in collagen, fibroblasts, and blood vasculature for all scaffolds. The collagen fibers and fibroblasts of the FT were oriented parallel to the long axis of the subcutaneous smooth muscle and the surface of the implant area.

The three scaffolds, CEM, GAxCEM, and GAxHV, used in this study were connective tissue derivatives and were composed of dense collagenous tissue with (GAxHV) or without (CEM and GAxCEM) their inherent porcine cells. CEM was processed in such a way that the inherent porcine cells are disrupted and washed out, resulting in a porous network. Our earlier study showed that CEM had surface porosity in the range of 13−846 nm, which is suitable for host tissue infiltration.[6] The GAxCEM prepared with 0.625% GA cross-linking concentration was also porous and supported host tissue infiltration. However, the

Scheme 1. Schematic Diagram Showing the Fields of View and Their Approximate Locations for (A) Thickness Measurements at 400× Magnification and (B) Volume Fraction (Tissue Components and Inflammatory Cells) as Well as Surface Density, Length Density, and Radial Diffusion Distance Estimations (Blood Vessels) at 1000× Magnification, and (C) Volume Fractions of Tissue Response Zones at 12.5× Magnification[a]

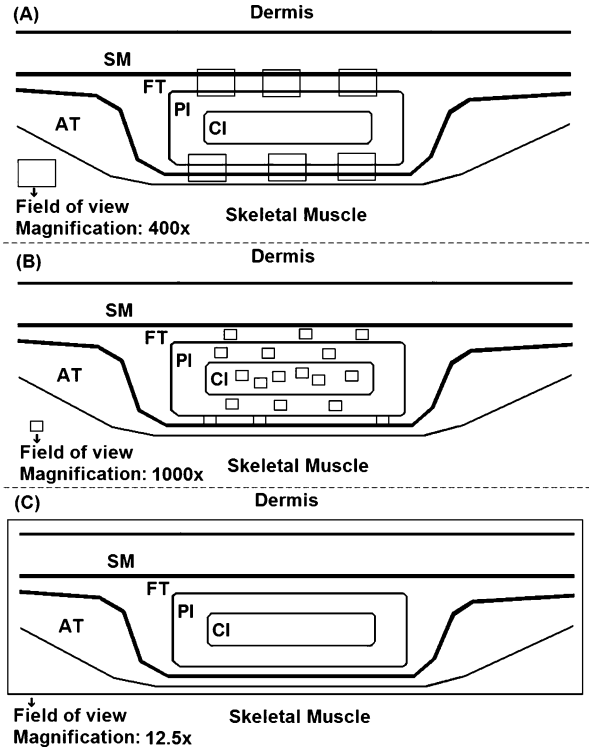

[a] SM − subcutaneous smooth muscle, FT − fibrous tissue surrounding the implant, PI − periphery of implant area, CI − core of implant area, and AT − adipose connective tissue.

compact arrangement of the collagen bundles and its inherent cells (Figure 2) made the GAxHV impermeable to host tissue infiltration.

At 21 days, the MT stained histology sections showed complete host tissue infiltration in the porous network of CEM, and the collagen of CEM was organized into dense bundles with random collagen fiber orientations (Figure 3A,B). The thickness and packing of the CEM collagen bundles varied between the core and periphery of the implant area. The bundles were thicker and less porous in the core of the implant area (CI) as compared to the thinner and highly porous organization in the periphery of the implant area (PI) (Figure 3A,B). The infiltrating host tissue was mainly composed of mononuclear cells and occasional giant cells restricted to PI. By 63 days, the dense collagen bundles of CEM were absent, and the implant area was composed of host adipose connective tissue (AT) with loose collagenous tissue containing adipose/fat cells (Figure 1B). However, in three of the eight CEM, implants at 63 days showed some residual inflammatory tissue (RT in Figure 3C) in addition to the AT in the implant area, and there was no evidence of any residual CEM.

The porous network structure of GAxCEM was also infiltrated completely with host tissue at both 21 (Figure 4A,B) and 63 (Figure 4C,D) days of implantation. The organization of collagen bundles of GAxCEM and host tissue in both CI and PI was similar to that observed with CEM, except that the thickness of the collagen bundles was similar for PI and CI of GAxCEM. However, the histological structure of GAxCEM 63 days was similar to that observed at 21 days, with collagen bundles of GAxCEM retaining their integrity (showing no apparent in vivo degradation) at 63 days. The host tissue infiltrate for GAxCEM at both 21 and 63 days was composed of mononuclear cells and some giant cells observed in PI.

The GAxHV scaffold was impermeable to host tissue infiltration, and the host tissue was thin and restricted to the PI at both 21 and 63 days as depicted in Figure 1E,F, respectively. The host tissue at the PI for GAxHV was also mainly composed of mononuclear cells with occasional giant cells. GAxHV also did not show any significant in vivo degradation by 63 days.

Tissue Response Zones at Subcutaneous Implantation Site. Figure 5A−F shows the polarized light microscopic images of pico-sirius red stained histology sections of the implant sites of the different scaffolds variants at 21 and 63 days of subcutaneous implantation in rats. Picro-sirius red stains collagen red on a pale yellow background in bright-field microscope, whereas under polarization microscope collagen appears bright orange-red, yellow, and/or bright green due to its anisotropic molecular organization under polarized light microscopy. The pico-sirius red staining further enhances collagen birefringence. The rest of the tissue appears pale/colorless at the site of implantation. As illustrated in Figure 5A−F and in Scheme 1, the subcutaneous implantation sites for all scaffold variants were categorized into three tissue response zones, fibrous tissue surrounding the implant (FT), periphery of the implant area (PI), and core of the implant area (CI). However, in the case of CEM at 63 days, the CI was considered absent because no intact collagen of CEM was detectable, and the entire implant area was designated as PI (Figure 5B). Furthermore, because host tissue failed to infiltrate into GAxHV, the entire CI for GAxHV, at both 21 and 63 days (Figure 5E,F), was designated as implant collagen (implant tissue also including inherent cells of HV) for the purpose of quantitative stereological analysis.

Quantitative Stereological Analysis: Implant Site Composition. In this study, volume changes of the tissue response zones in relation to each other have been good indicators for the rapid in vivo degradation of CEM. Significant decreases in the V_v of implant area in relation to fibrous tissue (Figure 6) and V_v of core in relation to periphery (Figure 7) from 21 to 63 days were observed for CEM at the subcutaneous level in a rat model. In contrast, from 21 to 63 days, no significant differences were observed for V_v of implant area to fibrous tissue (Figure 6) and V_v of core to periphery (Figure 7) in the case of GA cross-linked controls, indicating that GAxCEM and GAxHV are effectively non-degradable in the time frame of 63 days.

Traditionally, the thickness of fibrous tissue surrounding the implant has been used as a measure for toxicity as well as chemical and/or mechanical irritation caused by the implanted scaffold to the surrounding tissue. The arithmetic thickness (T_a) was less than 52 μm for all scaffolds, and no statistical differences were observed within or between the groups and time points, suggesting that no drastic effects, due to either toxicity or chemical/mechanical irritation, were caused by any of the scaffolds.

Tissue Composition. The relative volumes of the tissue components, collagen, nuclei, cytoplasm, and blood vessels, were utilized, in this study, to evaluate the severity of host inflammatory response.

Fibrous Tissue Surrounding Implant. As illustrated in Figure 8A, collagen was the main component (V_v between 50% and 75%) of the fibrous tissue surrounding the implant for all of the scaffolds. From 21 to 63 days, although not statistically significant, an increase in collagen content was observed for all scaffolds, indicating maturation of the fibrous connective

Table 2. Morphological Criteria for Cell Identification on H&E Stained Histology Sections Used in This Study

cell type	abbreviation	morphological criteria
fibroblasts[a]	Fb	ovoid nuclei in a spindle/stellate-shaped cell, variably euchromatic
fibrocytes	Fc	elongated dark stained (heterochromatic) nucleus in spindle-shaped cells with scant cytoplasm
lymphocytes	Lc	round to oval and variable sized nucleus depending on the cell size; often heterochromatic nuclei; sparse cytoplasm
plasma cells	PC	eccentrically placed nucleus within a round to ovoid cell; area nearnucleus pale/unstained; cartwheel/clock-like appearance of heterochromatin in nucleus
neutrophils	Np	segmented, with distinct narrowing of nuclei lobes and outline − mostly scalloped/jagged in horse; variably heterochromatic nucleus; colorless or pale eosionophilic staining of cytoplasm
eosinophils	Ep	distinctly segmented but less lobulated than neutrophils and often bilobed nucleus, with dark eosinophilic staining of cytoplasm
monocytes	Mc	often eccentrically positioned and variably shaped nucleus; slightly indented/ U-shaped/kidney-shaped/trilobed in a cloverleaf manner-shaped nucleus; pale cytoplasm
giant cells	GC	large cell with large number of nuclei and pale cytoplasm
other mononuclear cells	OMC	unidentified mononuclear cells;[b] adipose cells (single large vacuole,flattened nucleus displaced to one side); macrophages (variable sizes; nucleus ovoid or kidney shaped, pale cytoplasm often in large quantity), mast cells[c] and basophils[c] (basophilic cytoplasm, staining blue with hematoxylin)

[a] The majority of fibroblasts observed in this study at the subcutaneous implantation site were spindle shaped; where stellate, the fibroblasts were distinguished from macrophages by the nature of non-branching elongated cytoplasmic processes against the short thick pseudopodia of macrophages; another distinguishing criterion was that the nucleus of macrophages is smaller and darker as compared to that of fibroblasts. [b] Mononuclear cells that were difficult to identify on the basis of the above listed criteria. [c] Mast cells and basophils were absent in all of the tissue response zones at the subcutaneous implantation site for all implant variants in this study.

tissue. V_v of 18−28% of the fibrous tissue was occupied by cell nuclei. A significantly higher V_v of nuclei was observed for GAxHV as compared to that observed for CEM at 21 days, suggesting a higher degree of inflammatory cells in the fibrous tissue surrounding GAxHV. Between the V_v of nuclei and cytoplasm, no significant differences were observed for all scaffolds. Furthermore, no significant differences were observed between scaffolds and time points for V_v of blood vessels.

Periphery of the Implant Area. Figure 8B illustrates the results for the V_v estimations of collagen nuclei, cytoplasm, and blood vessels in the periphery of the implant area. At both 21 and 63 days, the V_v of collagen was lower than that observed for nuclei for all scaffolds, indicating the significant presence of inflammatory cells in the periphery of the implant area. No statistical differences were observed for the V_v of collagen as well as nuclei among the scaffolds and the time points, except for the V_v of collagen at 63 days between GAxHV and GAxCEM. GAxHV had a significantly lower V_v of collagen as compared to that of GAxCEM, which can be attributed to the absence of implant collagen in the periphery of GAxHV resulting from the failure of host tissue to penetrate into GAxHV. The collagen in the periphery of implant area for CEM at 21 days and GAxCEM at both 21 and 63 days was mainly the remains of the dense implant collagen, while that for CEM at 63 days was that of host connective tissue that replaced CEM. The V_v of cytoplasm was significantly higher that the rest of the scaffolds, indicating significant presence of cells with abundant cytoplasm like macrophages at both 21 and 63 days for all scaffolds. The V_v of blood vessels was maximum for CEM and minimum for GAxHV.

Core of the Implant Area. Figure 8C shows the results for the tissue composition of the core of the implant area. The significant presence of collagen for all scaffolds and time points, except for CEM at 63 days, is indicative of the remains of the implanted scaffolds at the subcutaneous level. At 21 days, the V_v of collagen was minimum for CEM and maximum for GAxHV, indicating rapid resportion of CEM. From 21 to 63 days, in the case of GAxCEM and GAxHV, no significant differences were observed for V_v of collagen, while the absence of collagen at 63 days for CEM demonstrated that CEM was completely absorbed. The presence/absence and the amount of nuclei, if present, are indicative of the degree of host tissue infiltration into the implanted scaffolds. Maximum V_v of nuclei for CEM suggested maximum host tissue infiltration into CEM, while the absence of host inflammatory cell nuclei within GAxHV at both 21 and 63 days indicated the failure of host tissue infiltration. A lower V_v of nuclei for GAxCEM at both 21 and 63 days is indicative of the rigidity of scaffold due to cross-linking. Higher V_v of cytoplasm was observed for all scaffolds when compared to that of V_v of nuclei. Blood vessels were absent in the core of the implant area for GAxCEM and GAxHV at 21 days. For GAxCEM, blood vessels were observed at 63 days.

Inflammatory Cell Distribution at Implant Site. The relative volumes of different cell nuclei were utilized to evaluate the distribution and nature of inflammatory cells in the different tissue response zones.

Fibrous Tissue Surrounding Implant. Fibrous tissue surrounding the implant is a loose connective tissue deposited by host in response to the introduction of the scaffold. Fibroblasts (Fb) and fibrocytes (Fc) are the primary cells of the fibrous tissue. However, a significant presence of inflammatory cells in the fibrous tissue can be indicative of the role of host tissue in the active removal of foreign material. The V_v estimations of the different cell nuclei in the fibrous tissue surrounding the implant are illustrated in Figure 9A. Fb constituted the majority of cells in the fibrous tissue at 21 days. However, by 63 days, the V_v of Fb decreased significantly for CEM and GAxHV, and that of Fc increased significantly for all scaffolds, suggesting a maturing fibrous tissue. The acute inflammatory cells, neutrophils (Np) and monocytes (Mc), were absent or $<0.5\%$ for all scaffolds at both 21 and 63 days. The majority of the chronic inflammatory cells were other mononuclear cells (OMC), especially macrophages. At 21 days, the V_v of OMC for the different scaffolds

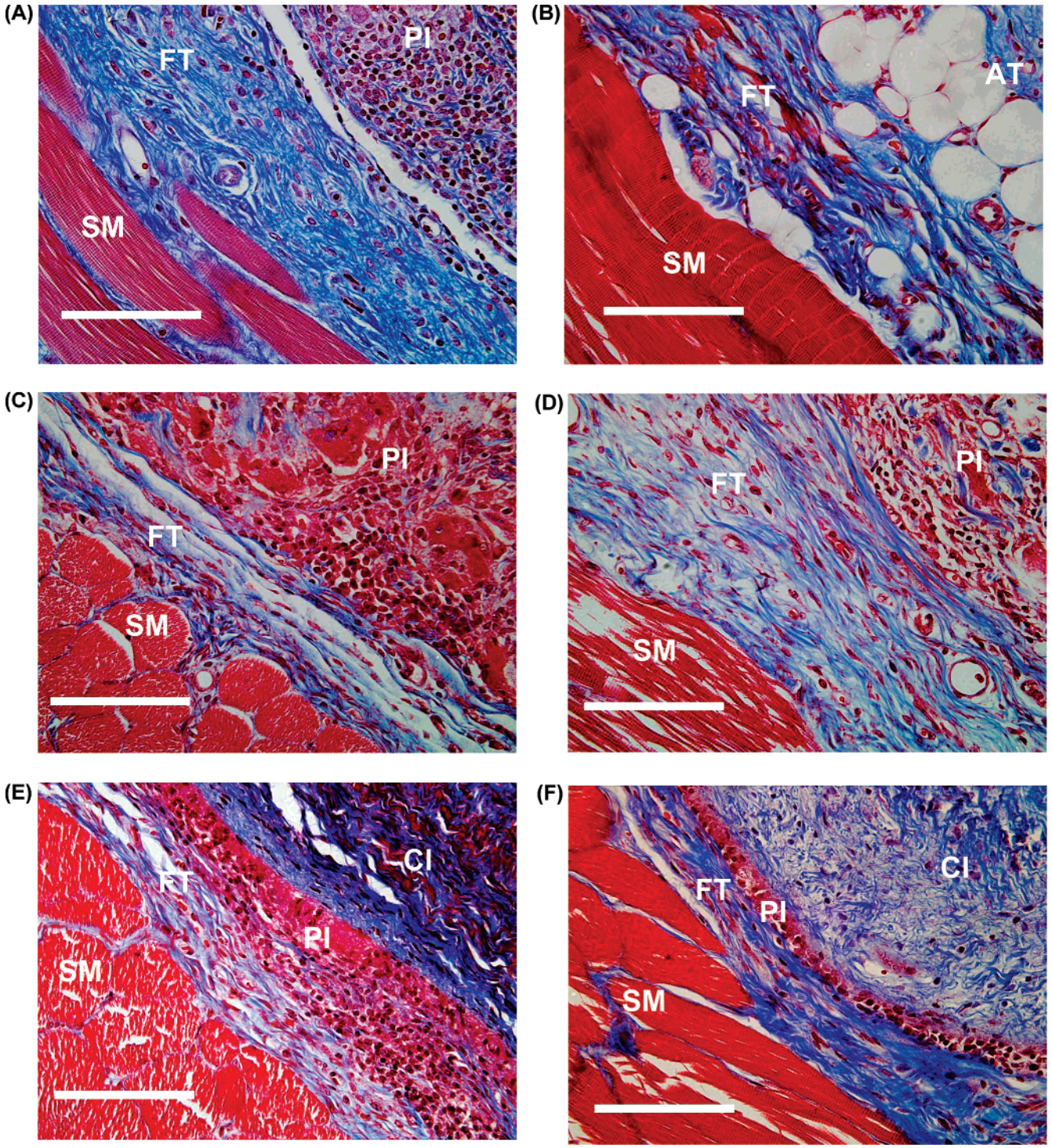

Figure 1. Light microscopic images of Masson's trichrome stained histology sections showing the fibrous tissue surrounding the implant (FT) for the scaffolds CEM (A,B), GAxCEM (C,D), and GAxHV (E,F) at time points 21 days (A,C,E) and 63 days (B,D,F). Notice the similar histological structure of the FT surrounding all scaffolds. It is composed of loose connective tissue rich in blood vasculature, fibroblasts, and collagen fibers (blue staining) running parallel to the subcutaneous smooth muscle (SM) tissue. PI − periphery of implant area, CI − core of implant area, AT − adipose connective tissue. The scale bar indicates 100 μm.

ranged between 35% and 50%, indicating an active role for host tissue in the degradation and removal of implanted scaffolds. From 21 to 63 days, the mean values for V_v of OMC decreased for all scaffolds, and the decrease was significant for GAxHV. Giant cells (GC) were absent at both 21 and 63 days for all scaffolds. Lymphocytes (Lc) were the majority of leukocytes in the fibrous tissue at 21 days. The mean value for V_v of Lc was maximum for CEM and minimum for GAxHV. However, at 63 days, the trend reversed and V_v of Lc increased significantly for GAxHV, suggesting immune reaction. Plasma cells (PC) were absent for all scaffolds except for CEM (~1%) at 21 days. Eosinophils (Ep) were absent in the fibrous tissue of CEM and GAxCEM at 21 days and <1% in the case of GAxHV. However, an increase in the V_v of Ep was observed at 63 days, and their V_v is maximum for GAxHV (about 7%) and minimum for CEM (<0.5%), and the differences were not statistically significant.

Periphery of the Implant Area. The periphery of the implant area is the location where the inflammatory cells are concentrated. Figure 9B presents the results for the V_v of different cell

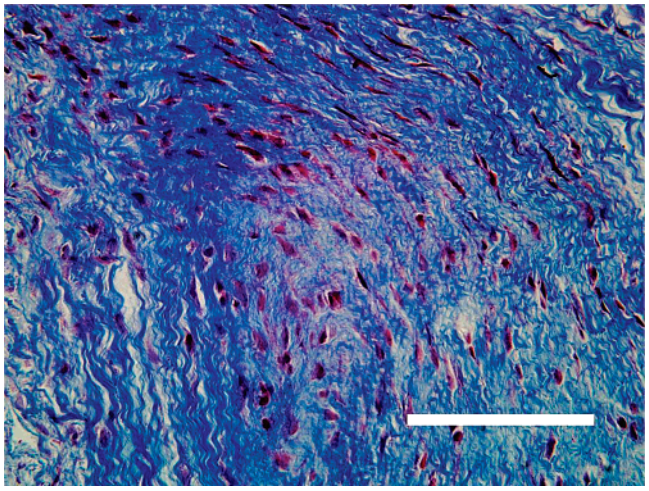

Figure 2. Masson's trichrome stained histology section showing the histological structure of the implant area of GAxHV. Notice the typical histological appearance of HV tissue with its inherent cells (fibroblasts) intact at 63 days after subcutaneous implantation. The scale bar indicates 100 μm.

nuclei at the periphery of implant area. Between 50% and 90% of the V_v of nuclei belonged to OMC at both 21 and 63 days, indicating an overall high volume of phagocytic activity. From 21 to 63 days, the V_v of OMC decreased, and the decrease was significant for GAxHV. On the other hand, an increase in the mean values for V_v of Fb, Lc, and PC was observed for GAxHV, and the increase was significant for V_v of Fb and PC, suggesting an increased immune response and Fb activity. Fc were absent in the periphery of implant area for all scaffolds. At both 21 and 63 days, the V_v of Lc and PC was minimal for GAxCEM, but not statistically different from CEM. At 21 days, Ep were absent for all scaffolds, while at 63 days, their V_v was $<0.5\%$ for CEM and GAxCEM and absent for GAxHV. The V_v of Np and Mc was $<2\%$ in the periphery of implant area. GC formation was observed for all scaffolds, and the values of V_v of GC nuclei were $<5\%$. Among the different scaffolds, GC formation was higher for GA cross-linked samples as compared to the non-cross-linked CEM.

Core of the Implant Area. Figure 9C presents the results for the cellular composition of the core of the implant area. Host cells failed to infiltrate into GAxHV at both 21 and 63 days, while the core of implant area was absent for CEM at 63 days. Among the cell nuclei, for CEM at 21 days and GAxCEM at both 21 and 63 days, OMC were the dominant cells. However, from 21 to 63 days, the V_v of OMC decreased significantly, while that of Fb in the case of GAxCEM increased. Fc were absent. The V_v of Lc and PC was significantly high for CEM at 21 days when compared to that of GAxCEM. The V_v of Lc for GAxCEM was low, and no statistical difference was observed for their values between 21 and 63 days, while PC were absent at both time points. Ep were absent for all scaffolds at both 21 and 63 days. The V_v of Np and Mc were absent or $<1\%$ in the core of implant area for the different scaffolds at both 21 and 63 days. GC were also absent in the core of the implant area for both CEM and GAxCEM.

Angiogenesis. The results for the stereological estimations of the surface density (S_v), length density (L_v), and radius of diffusion (R_{diff}) of blood vessels and capillaries in the different tissue response zones are shown in Figure 7A−C. The higher are the S_v and L_v, and lower is the R_{diff}, and the more vascular is the tissue. Among the scaffolds, similar trends were observed for S_v and L_v estimations in the different tissue response zones.

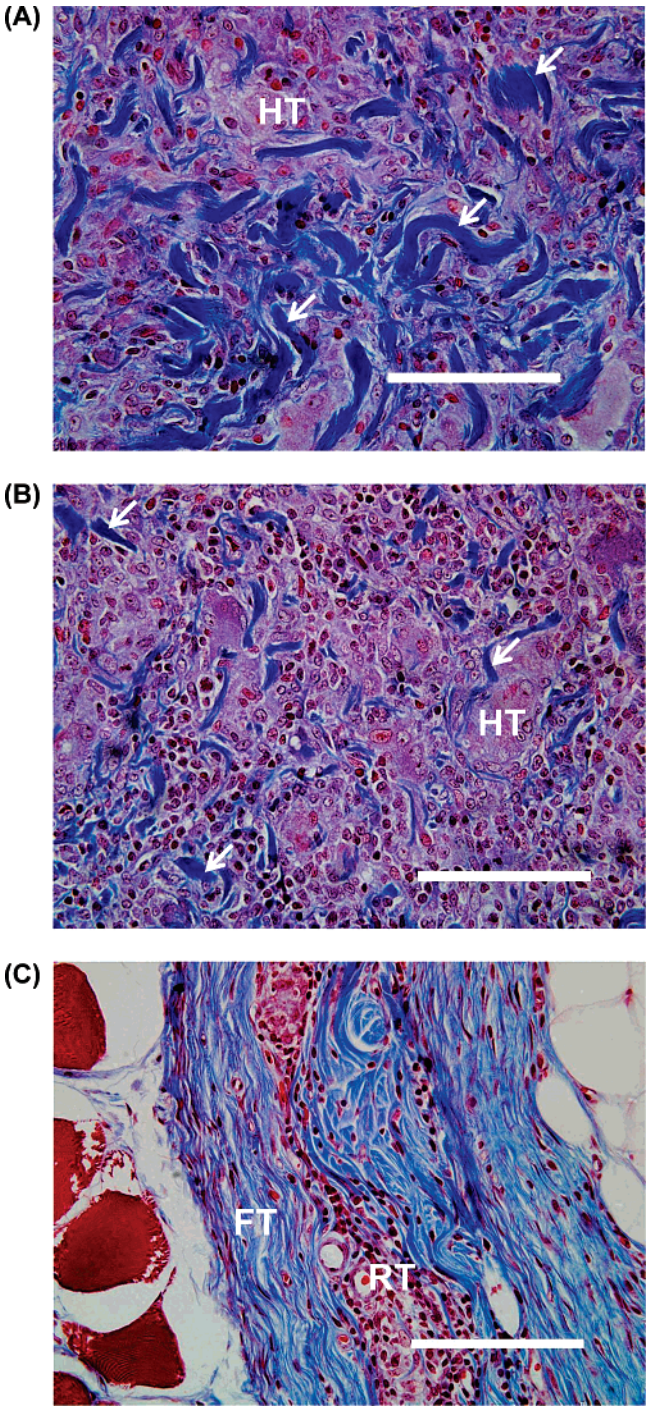

Figure 3. Masson's trichrome stained light micrographs showing the histological structure at the subcutaneous implantation site of CEM at 21 days (A,B) and 63 days (C). (A) Core of implant area − notice the randomly oriented dense collagen bundles (blue color indicated by arrows) of CEM infiltrated with host tissue (HT). (B) Periphery of implant area − the collagen bundles (indicated by arrows) are thinner as compared to the core of implant area, indicating faster resorption. (C) The CEM implantation site at 63 days showing the residual inflammatory tissue (RT) and the absence of the randomly oriented dense bundles of collagen seen at 21 days. FT − fibrous tissue. The scale bar indicates 100 μm.

Fibrous Tissue Surrounding Implant. At 21 days, the S_v and the L_v were minimum for CEM and maximum for GAxHV (Figure 10A,B). From 21 to 63 days, no statistical differences in the values for S_v and L_v were observed for each of the scaffolds. However, at 63 days, the S_v and L_v for GAxHV were significantly higher than those observed for CEM (Figure 7A,B).

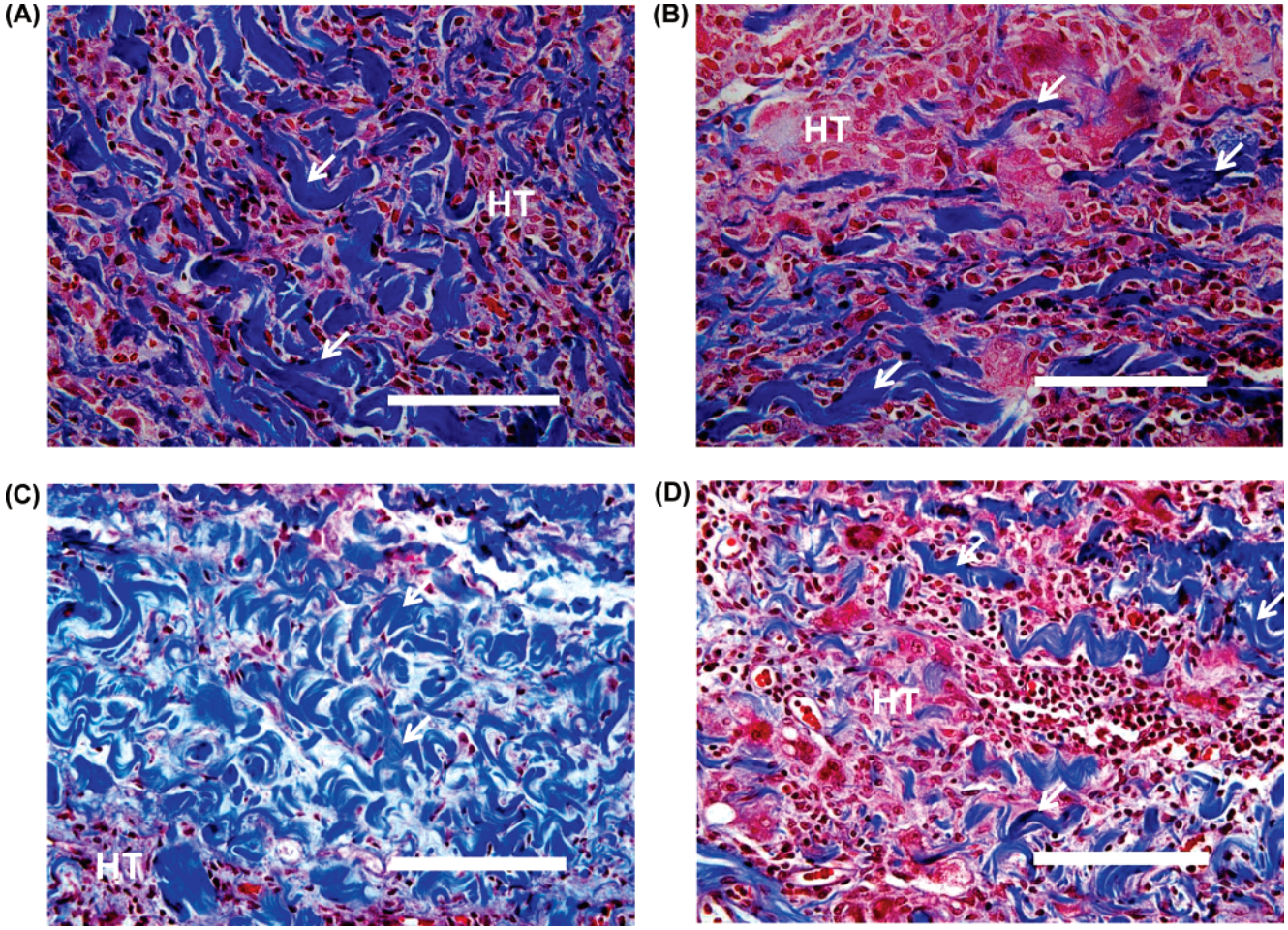

Figure 4. Masson's trichrome stained light micrographs showing the histological structure at the subcutaneous implantation site of GAxCEM at 21 days (A,B) and 63 days (C,D). Host tissue infiltration reached the core of the implant area (A,C) and was dense in the periphery of implant area (B,D) as compared to the core of implant area. Notice that the collagen bundles (blue color indicated by arrows) are thick both at the core as well as at the periphery of the implant area and do not show any apparent resorption even after 63 days (C,D) at the subcutaneous implant site. The scale bar indicates 100 μm.

The inter-blood vessel R_{diff} was maximal for GAxCEM, which was significantly higher than that observed for GAxHV at 21 days (Figure 10C). Between the time points, the R_{diff} values were similar for CEM and GAxHV, while that for GAxCEM showed a significant decrease (Figure 7C).

Periphery of the Implant Area. The S_v and L_v were minimal for GAxCEM and maximal for GAxHV at 21 days, and the difference was significant between GAxCEM and GAxHV (Figure 10A,B). On the other hand, at 63 days, the values for S_v and L_v were minimum for GAxCEM and maximum for CEM, and, as compared to that at 21 days, an increase in S_v and L_v was observed for GAxCEM and CEM, while that for GAxHV did not change significantly (Figure 10A,B). In addition, the R_{diff} was significantly higher for GAxCEM at 21 days when compared to that of CEM as well as GAxHV (Figure 10C). By 63 days, the R_{diff} decreased significantly for GAxCEM, while no statistical difference was observed for both CEM and GAxHV.

Core of the Implant Area. The S_v and L_v values for CEM were significantly higher than those observed for GAxCEM and GAxHV (Figure 10A,B). No blood vessels were observed in the core of GAxHV scaffold, and the values for S_v and L_v for GAxCEM were significantly low as compared to those for CEM. The R_{diff} was minimal for CEM, which was significantly lower than that observed for GAxCEM and GAxHV at both 21 and 63 days (Figure 10C).

Discussion

Tissue responses to scaffolds vary depending on the properties, such as chemical inertness or reactivity (antigenicity/bioactive nature), surface texture, micro-architecture, and biodegradability/solubility, and also on the duration of implantation.[14,16,29−31] The three matrices used in this study, CEM, GAxCEM, and GAxHV, are xenogenic connective tissue derivatives, and they differ from each other in their composition and/or matrix architecture. CEM and GAxCEM are decellularized porous scaffold with mesh-like architecture, while GAxHV is nonporous and contained the inherent cells of the porcine HV.

The native CEM was completely infiltrated with host tissue at 21 days (Figure 5A), and by 63 days the scaffold was absorbed and replaced by host tissue (Figure 5B). GAxCEM was also infiltrated with host tissue (Figure 5C,D). However, the amount of host tissue infiltrating into GAxCEM, as indicated by the V_v estimations of collagen in the core of the implant area (Figure 5A), was significantly lower than that observed for CEM. On the other hand, host tissue failed to infiltrate into GAxHV (Figure 5E,F).

The rapid and uniform host tissue infiltration into the CEM can be attributed to its biological origin, porous mesh-like architecture, and rapid biodegradation, based on the fact that ECM contains cell adhesion receptors and 3D architecture, which mediate a range of different cell functions such as cell

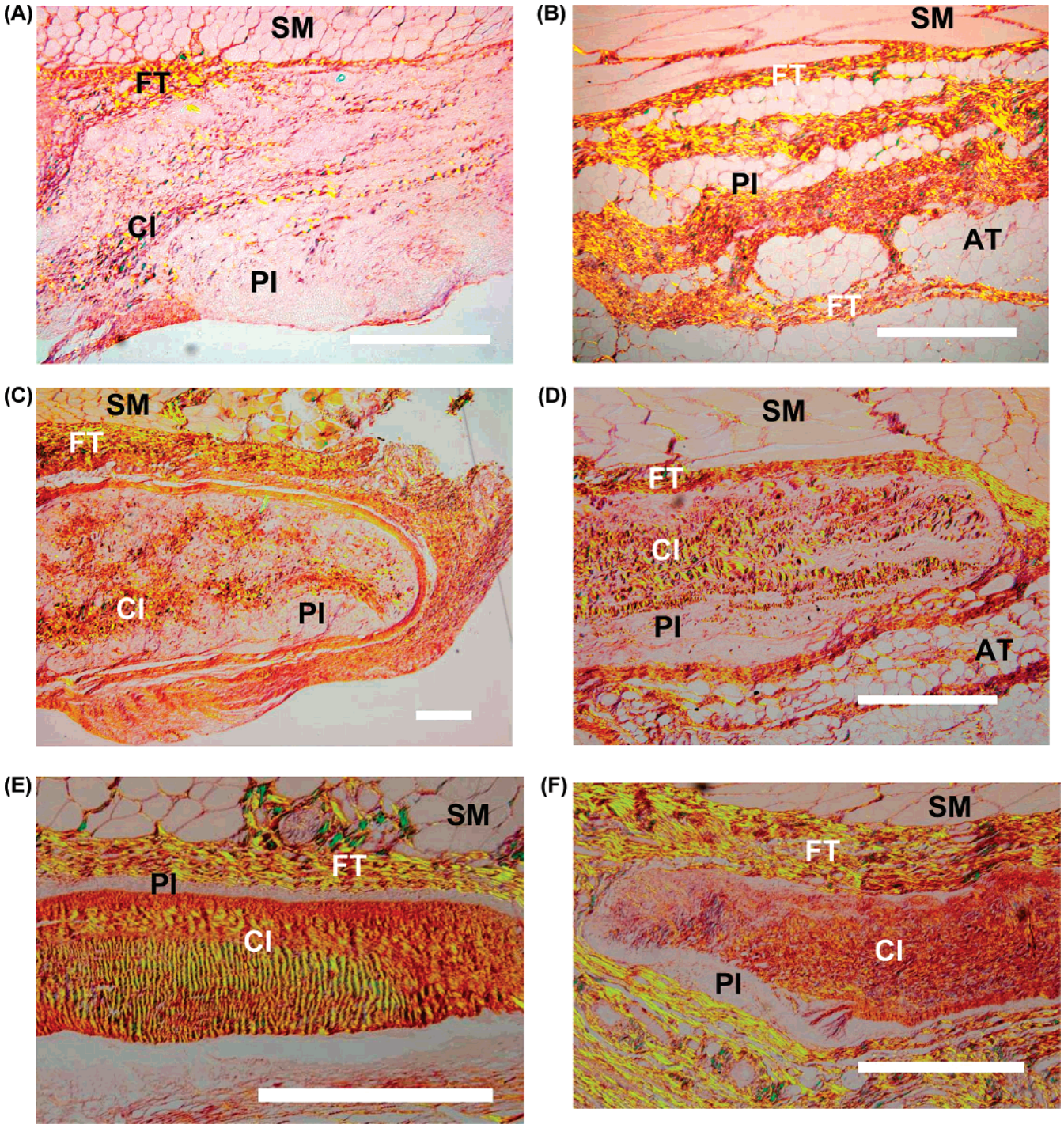

Figure 5. Polarized light microscopic images of the subcutaneous implantation sites distinguishing bifringent collagen (red, yellow, and green colors) from the rest of the tissue components (pale/dull colors) on picosirus red stained histology sections of CEM (A,B), GAxCEM (C,D), and GAxHV (E,F) at 21 days (A,C,E) and 63 days (B,D,F). The classification of tissue response zones into FT − fibrous tissue surrounding the implant, PI − periphery of the implant area, and CI − core of the implant area is based on the nature and distribution of collagen and host tissue at the subcutaneous implantation site (details in text). SM − subcutaneous muscle, AT − adipose connective tissue. Scale bar indicates 400 μm.

attachment and polarity, growth and differentiation, adhesion, migration, and tissue remodelling.[32−38] Porosity plays an important role in the host tissue infiltration into an implanted matrix, and cross-linking reduces the porosity, while increasing the stiffness of the matrix. In the case of GAxCEM, prior to cross-linking, the matrix was processed in such a way that its inherent cells were disrupted and removed, and the resulting matrix had a loose fibrous mesh-like architecture.[6−8] Apparently, GA cross-linking did not reduce the porosity of CEM enough to exclude GAxCEM from host tissue infiltration (Figure 4A−D). In contrast, the HV samples were processed in such a way that their in situ constitution is preserved, which resulted in a nonporous scaffold that was impervious to tissue infiltration (Figure 2).

V_v estimations for the different tissue response zones (Figures 6 and 7) demonstrated the in vivo degradation of native CEM scaffold. A significant decrease in the implant area (Figure 6) from 21 to 63 days and the near normal histological structure observed at the subcutaneous implantation site (Figure 5B) at 63 days illustrated the complete absorption of native CEM

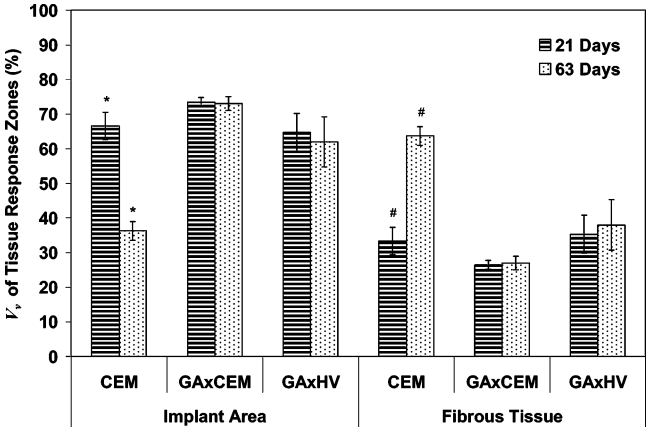

Figure 6. Volume fraction (V_v) estimations of the implant area and the fibrous tissue as a function of total volume of the subcutaneous implantation site (implant area + fibrous tissue). "*" and "#" indicate statistical difference ($p < 0.05$).

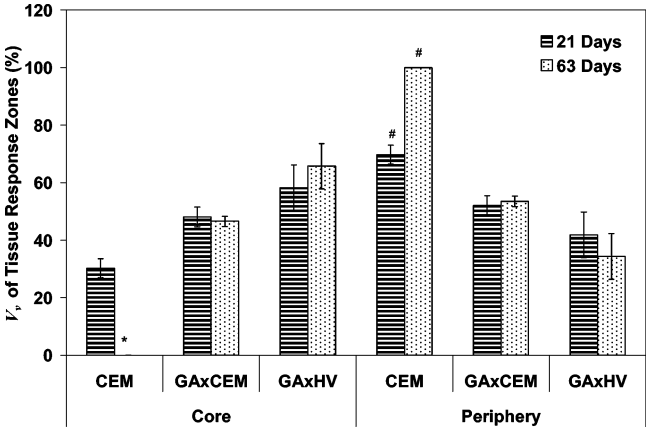

Figure 7. Volume fraction (V_v) estimations of the core and periphery of the implant area as a function of total volume of the implant area. "*" and "#" indicate statistical difference ($p < 0.05$).

within 63 days. No apparent degradation was observed for both GAxCEM and GAxHV scaffolds within the study period. Collagen-based scaffolds have often been cross-linked to make them resistant to in vivo degradation.[39] However, losses of collagen were reported for similar materials, derived from xenogenic dermal tissue.[40] Furthermore, degradation of polymeric GA derived cross-links has been reported, which could result in the leaching of low as well as of high molecular weight degradation products from GA fixed tendons.[41] Hence, there can be some degradation of both GAxCEM and GAxHV. Yet the determination of the extent of degradation would require better quantitative evaluations.

Calcification is a common problem associated with clinically available heart valve prostheses, and significant efforts have been directed to reduce the calcification potential of existing scaffolds. Two commonly recognized factors causing calcification are GA cross-linking and remnants of xenogenic cellular materials, and their role in calcification has been reviewed earlier.[5] Both GA cross-linking and cellular materials are thought to provide nucleation sites for calcium attachment leading to calcification.[5] In the current study, GA cross-linking and nondecellularized porcine HV have been used as negative controls and were expected to cause calcification. However, none of the implants showed any signs of calcification during the study period. The reasons for no calcification can only be speculated because the exact mechanisms of calcification are not known. Earlier studies on posttreatment of 0.625% GA cross-linked

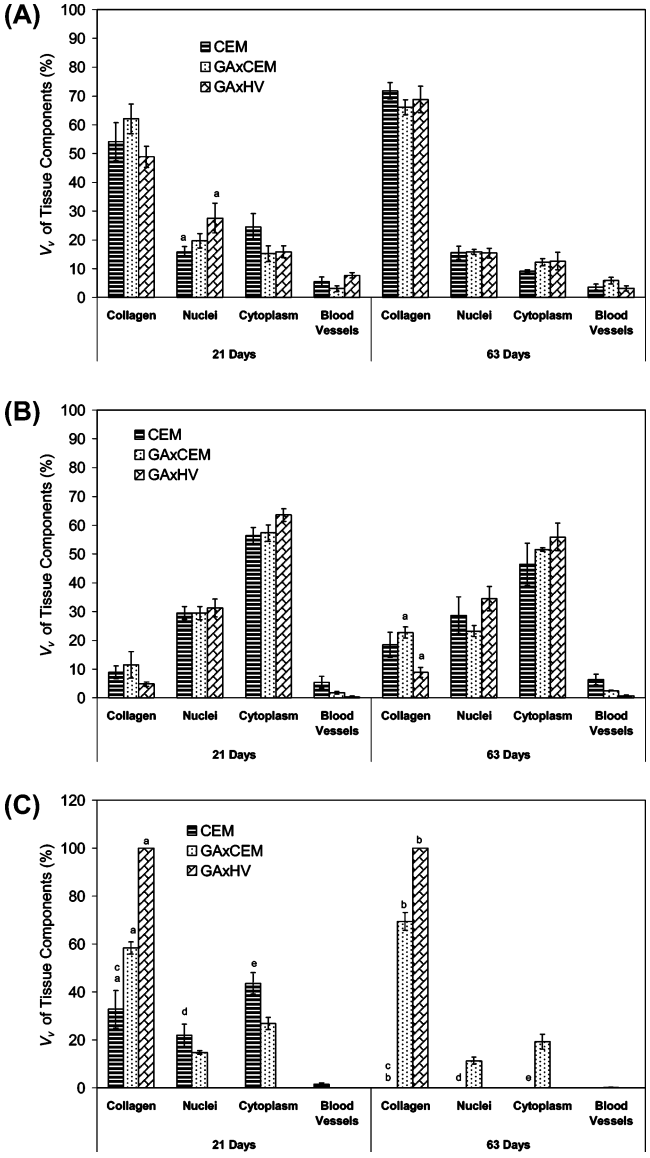

Figure 8. Volume fraction (V_v) estimations of the tissue components collagen, nuclei, cytoplasm, and blood vessels as a function of total volume of the tissue response zones: (A) fibrous tissue surrounding the implant, (B) periphery of implant area, and (C) core of the implant area respectively. "a", "b", "c", "d", and "e" indicate statistical difference ($p < 0.05$).

pericardium/HV with chitosan or partially degraded heparin were shown to prevent calcification in rat subcutaneous model.[42,43] Similarly, posttreatments (sterilization) of the scaffolds, in the current study, with peracetic acid and penicillin−streptomycin solutions might have some role in the attenuation of calcification.

All three matrices used in this study were surrounded by fibrous tissue. The formation of fibrous tissue in the case of fibro-porous scaffolds has been reported to depend on the microarchitecture of the scaffold.[16] According to Sanders et al., thresholds of fiber diameter (2.0−5.9 μm), pore sizes (0.8−8.0 μm), and fiber spacing (30−60 μm) existed for polycarbonate-urethane/single fiber polypropylene implants, within which the fibrous tissue surrounding the scaffold does not form.[16] However, deviations from these ranges can occur. CEM has been shown to have nanoscale architecture, with mean fiber diameters ranging between 29 and 219 nm, pore diameters between 13 and 846 nm, and pore elevations between 67 and 1003 nm.[6] The formation of fibrous tissue surrounding CEM, observed in this study, can be attributed to the high variability in its sub-

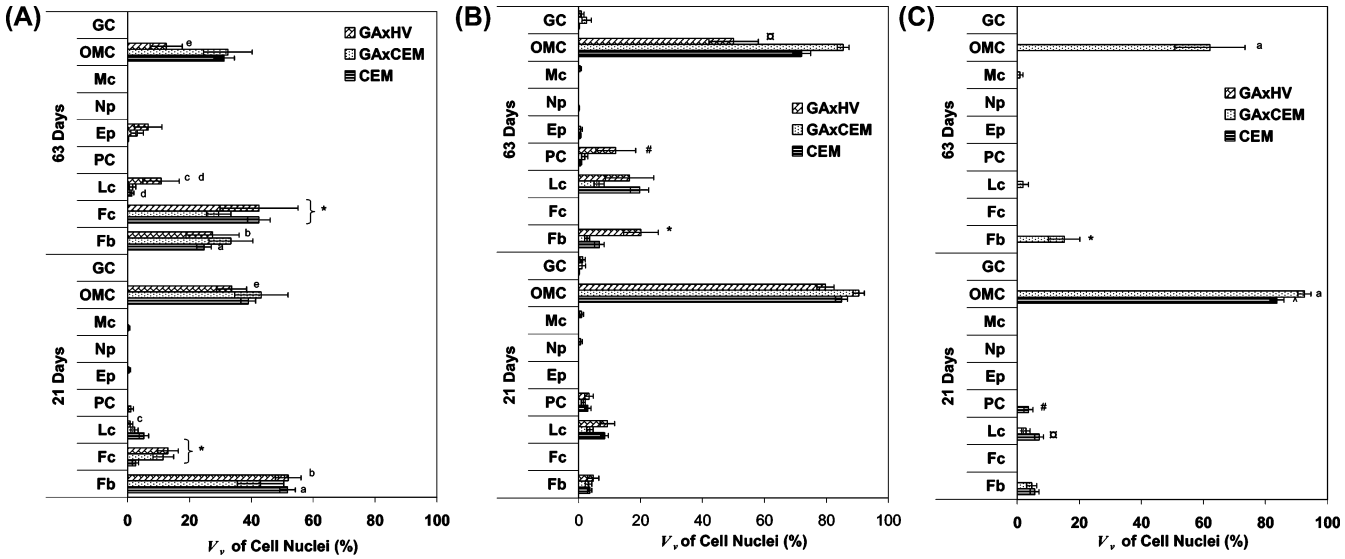

Figure 9. Volume fraction (V_v) estimations of cellular components, cell nuclei of each cell type (Fb − fibroblasts, Fc − fibrocytes, Lc − lymphocytes, PC − plasma cells, Ep − eosinophils, Np − neutrophils, Mc − monocytes, OMC − other mononuclear cells, and GC − giant cells), as a function of volume of the total cell nuclei present in (A) fibrous tissue surrounding the implant, (B) periphery of implant area, and (C) core of the implant area. "a", "b", "c", "d", "e", "f", "*", "#", "∧", and "○" indicate statistical difference ($p < 0.05$).

micrometer scaffold architecture as well as its reactivity. Collagenous materials have been reported to elicit giant cell formation,[40] and the release of enzymes into the extracellular spaces by the GC could trigger the formation of fibrous tissue to protect the surrounding host tissue from degeneration due to lysozomal enzymes. A similar explanation can be used to explain the formation of fibrous tissue surrounding GAxCEM and GAxHV. However, GA cross-linking as well could have a significant role in the formation of fibrous tissue surrounding GAxCEM and GAxHV.

About 25−40% of the implantation site was fibrous tissue for all scaffolds, except CEM at 63 days (Figure 6). In the case of CEM, the V_v of fibrous tissue increased significantly from 21 to 63 days. The significant increase in V_v of fibrous tissue at the implantation site for CEM at 63 days was not due to an actual increase in the volume of the fibrous tissue, but due to a relative significant decrease in the volume of the implant area. In addition, it is interesting to note that even after remodeling of the implant area for CEM at 63 days, the thickness of the fibrous tissue surrounding the implant did not show a statistical difference from that observed at 21 days. CEM underwent bulk degradation (Figure 3A,B). New host tissue constituting of adipose connective tissue with loose fibrous tissue interspersed with adipose/fat cells was deposited in place of the resorbed CEM scaffold. The original fibrous tissue surrounding the implant was distinct and distinguishable from the rest of the tissue (Figure 5C). Between 21 and 63 days, in the case of GAxCEM and GAxHV, the V_v and the T_a estimations for the fibrous tissue did not show significant differences, indicating that a steady state for tissue response has been reached by 21 days and sustained through to 63 days.

V_v estimations for the tissue components demonstrated that collagen is the major constituent of the fibrous tissue surrounding all scaffolds (Figure 8A). At 21 days, an active fibrous tissue predominantly containing fibroblasts was observed. A significant increase in fibrocytes at 63 days indicated a maturing fibrous tissue for all scaffolds. However, the significant presence of fibroblasts and inflammatory cells, mainly OMC, in the fibrous tissue of all scaffolds indicated that the fibrous tissue was still active at 63 days, although to a lesser degree as compared to that at 21 days.

Acute inflammatory cells were absent or <1% in all of the tissue response zones at both 21 and 63 days, indicating the resolution of acute inflammation early during the implantation. The acute inflammatory response to similar materials has been reported to be resolved within 7 days of implantation.[40,44] In the current study, the appearance of eosinophils in the fibrous tissue surrounding the implant was observed at 63 days. The role of eosinophils in immune response to biomaterials/tissue engineering scaffolds is not clear. Eosinophils have been reported to be one of the cells that may be present in the acute inflammatory phase.[45] In disease states, eosinophils have also been reported to have some role in hypersensitivity reactions.[46,47] However, the absence of mast cells and basophils, the main cells associated with hypersensitivity reactions, indicated the absence of hypersensitivity reactions during the study period with all of the scaffolds used in this studied. Eosinophils were absent in the fibrous tissue surrounding CEM at 21 days, and their V_v at 63 days was less than 0.2%. Higher V_v of eosinophils in the case of GAxCEM and GAxHV could indicate some role of GA cross-linking in the recruitment of eosinophils.

Chronic inflammatory phase in the periphery and the core of implant area was dominated by OMCs, mainly macrophages. The significantly higher V_v of cytoplasm also indicates the significant presence of macrophages. Macrophages have been reported to play an important role in tissue response to foreign materials, including phagocytosis, antigen presentation, resorption of the scaffolds, wound repair, and tissue reorganization.[48,49] The high V_v of OMCs indicated the active role played by macrophages in the absorption of CEM and the remodeling of the implant site at 63 days. The macrophages are also known to control fibroblast activity, thus indirectly effecting the formation of collagen.[50,51] Significant V_v of fibroblasts was observed in the periphery of GAxHV and in the core of GAxCEM at 63 days, indicating the fibroblast mediated deposition/remodeling of connective tissue. Fibrocytes were absent for all scaffolds in the implant area. Giant cells, indicating the fusion of activated macrophages, were also observed for all scaffolds except CEM at 63 days, and their V_v was higher for the GA cross-linked samples. Immune cells, lymphocytes and plasma cells, have been observed for all scaffolds in the implant area. Initially (at 21 days), lymphocytic response was higher in

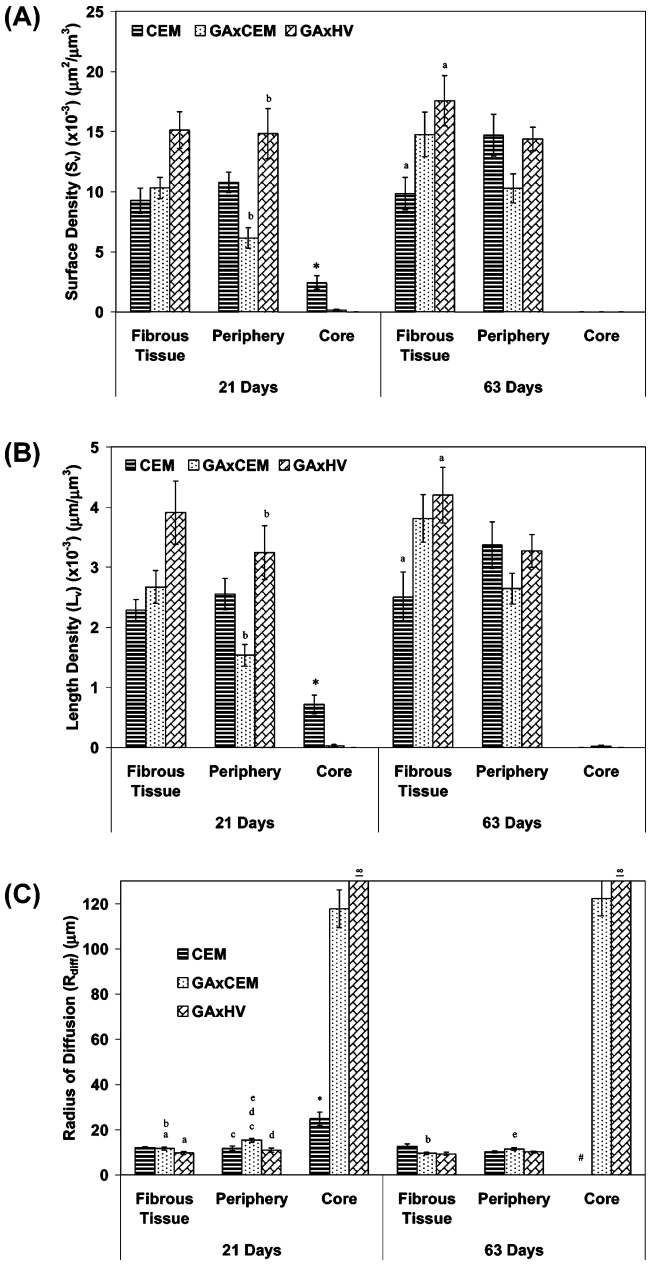

Figure 10. Angiogenesis. (A) Surface density (S_v) of blood vessels, (B) length density (L_v) of blood vessels, and (C) inter-blood vessel radius of diffusion (R_{diff}) distance in the different tissue response zones. "a", "b", "c", "d", "e", "*", and "#" indicate statistical difference ($p < 0.05$), while ∞ indicated infinity.

the case of CEM, which subsided by 63 days. However, at 63 days the lymphocytic response was higher for the GA cross-linked samples, especially GAxHV. The increase in the lymphocytic response in the GA cross-linked samples later during the implantation could indicate antigen presentation by macrophages.

Establishment of vasculature is essential for the exchange of blood, oxygen, nutrients, and waste products with the host tissue infiltrating into the scaffold matrix. Angiogenesis/neo-vascularization associated with implanted biomaterials/scaffolds can depend on at least three different parameters, bioactive nature of the scaffold,[52] porosity of the scaffold,[53] and the metabolic activity of the infiltrating host tissue.[54] The stereological estimations of S_v, L_v, and R_{diff}, in this study, indicated that angiogenesis/neo-vascularization, in fact, depended on the bioactive nature and porosity of scaffold as well as on metabolic activity of the infiltrating host tissue (Figure 10A−C). CEM is a bioactive and porous scaffold that facilitated complete and uniform infiltration of host tissue, resulting in a well-spread blood vascular network at the implantation site. In the case of GAxCEM, the bioactivity and porosity of CEM were restricted by GA cross-linking, which resulted in a lesser degree of host tissue infiltration and neo-vascularization into the scaffold as compared to that for CEM. From 21 to 63 days, S_v and L_v increased, while R_{diff} decreased significantly for GAxCEM, indicating an increased cellular activity, probably indicating degradation and antigen presentation by macrophages. An increase in macrophage population/activity has been reported to increase vascularization.[54] In the case of GAxHV, GA cross-linking excluded the GAxHV matrix from host tissue infiltration and neo-vascularization. However, accumulation of host tissue at the exterior/periphery of the GAxHV scaffold resulted in high density of host cells, which could be the reason for a higher degree of angiogenesis at periphery as well as fibrous tissue as compared to that observed for CEM. Furthermore, the results for L_v estimations of blood vasculature in all of the tissue response zones for all of the scaffolds were similar to those observed for S_v, indicating that the blood vessels are less tortuous, and any increase in the S_v and L_v can be due to branching or increase in volume of existing vasculature.[55]

In summary, CEM is an ECM derivative, and its insertion at the subcutaneous level in rats promoted a rapid host tissue infiltration, resorption of the implant, and the eventual remodeling of the subcutaneous implantation site. GA cross-linking of CEM resulted in a reduced amount of host tissue infiltration and angiogenesis, and also a drastic reduction in degradation rate. Furthermore, the inherent tissue architecture and stabilization by GA cross-linking caused the failure of host tissue to infiltrate into the matrix of GAxHV. Acute inflammatory response was resolved early during implantation of all scaffolds, while chronic inflammatory response was predominated by macrophages except for CEM at 63 days. Giant cell formation was observed restricted to the periphery of the implant area for all scaffolds, but to a greater degree in GA cross-linked controls. Lymphocytic response appeared to be influenced by the rate of in vivo degradation of the implant. Angiogenesis/neo-vascularization depended on the porosity of scaffold as well as on metabolic activity of the infiltrating host tissue. Having characterized the basic in vivo life and behavior of the rapid degrading non-cross-linked decellularized CEM, future research would involve tailoring of properties of CEM to specific soft tissue reconstruction applications, functional in vivo efficacy studies, as well as comparisons with commercially available materials.

Acknowledgment. We would like to thank Yolanda Garcia for her assistance in the surgery. This work was funded by an Enterprise Ireland −Technology Development grant.

Abbreviations

AT, adipose connective tissue
CEM, cholecyst-derived extracellular matrix
CI, core of implant area
ECM, extracellular matrix, extracellular matrices
Ep, eosinophils
Fb, fibroblasts
Fc, fibrocytes
FT, fibrous tissue surrounding implant
GA, glutaraldehyde
GAxCEM, glutaraldehyde crosslinked cholecyst-derived extracellular matrix

GAxHV, glutaraldehyde crosslinked heart valve
GC, giant cells
H&E, hematoxylin and eosin
HV, heart valve(s)
I, number of intersections between object of interest and test line
L, length (measured thickness)
Lc, lymphocytes
L_T, total length of test line
L_v, length density, length per unit volume
MT, Masson's trichrome
Mc, monocytes; PC, plasma cells
PI, periphery of implant area
Np, neutrophils
OMC, other mononuclear cells
P_P, partial points, number of points falling on object of interest
P_T, test points; number of points falling on reference space
R_{diff}, radial diffusion distance between blood vessels
RT, residual inflammatory tissue
SM, subcutaneous muscle
S_v, surface density, surface area per unit volume
T_a, arithmetic thickness
T_s, thickness of section
V_v, volume density, volume fraction, volume per unit volume

References and Notes

(1) Hubbell, J. A. *Curr. Opin. Biotechnol.* **2003**, *14*, 551−558.
(2) Shin, H.; Jo, S.; Mikos, A. G. *Biomaterials* **2003**, *24*, 4353−4364.
(3) Badylak, S. F. *Transplant. Immunol.* **2004**, *12*, 367−377.
(4) Badylak, S. F. *Semin. Cell Dev. Biol.* **2002**, *13*, 377−383.
(5) Schmidt, C. E.; Baier, J. M. *Biomaterials* **2000**, *21*, 2215−2231.
(6) Burugapalli, K.; Thapasimuttu, A.; Chan, J. C. Y.; Yao, L.; Brody, S.; Kelly, J. L.; Pandit, A. *Biomacromolecules* **2007**, *8*, 928−936.
(7) Coburn, J. C.; Brody, S.; Billiar, K. L.; Pandit, A. *J. Biomed. Mater. Res.* **2007**, *81A*, 250−256.
(8) Brody, S.; McMahon, J.; Yao, L.; O'Brien, M.; Dockery, P.; Pandit, A. *Biomaterials* **2007**, *28*, 1461−1469.
(9) Bigi, A.; Cojazzi, G.; Panzavolta, S.; Rubini, K.; Roveri, N. *Biomaterials* **2001**, *22*, 763−768.
(10) Parker, J. A.; Walboomers, X. F.; Von Den Hoff, J. W.; Maltha, J. C.; Jansen, J. A. *Tissue Eng.* **2003**, *9*, 117−126.
(11) Akers, J. M.; Peckham, P. H.; Keith, M. W.; Merritt, K. *IEEE Trans. Rehab. Eng.* **1997**, *5*, 207−220.
(12) Soiderer, E. E.; Lantz, G. C.; Kazacos, E. A.; Hodde, J. P.; Wiegand, R. E. *J. Surg. Res.* **2004**, *118*, 161−175.
(13) Loebsack, A.; Greene, K.; Wyatt, S.; Culberson, C.; Austin, C.; Beiler, R.; Roland, W.; Eiselt, P.; Rowley, J.; Burg, K.; Mooney, D.; Holder, W.; Halberstadt, C. *J. Biomed. Mater. Res.* **2001**, *57*, 575−581.
(14) Sanders, J. E.; Stiles, C. E.; Hayes, C. L. *J. Biomed. Mater. Res.* **2000**, *52*, 231−237.
(15) Holder, W. D., Jr.; Gruber, H. E.; Moore, A. L.; Culberson, C. R.; Anderson, W.; Burg, K. J.; Mooney, D. J. *J. Biomed. Mater. Res.* **1998**, *41*, 412−421.
(16) Sanders, J. E.; Lamont, S. E.; Mitchell, S. B.; Malcolm, S. G. *J. Biomed. Mater. Res.* **2005**, *72A*, 335−342.
(17) Klinge, U.; Schumpelick, V.; Klosterhalfen, B. *Biomaterials* **2001**, *22*, 1415−1424.
(18) Burugapalli, K.; Koul, V.; Dinda, A. K. *J. Biomed. Mater. Res.* **2004**, *68A*, 210−218.
(19) Ye, Q.; Ohsaki, K.; Ii, K.; Li, D. J.; Zhu, C. S.; Yamashita, Y.; Tenshin, S.; Takano-Yamamoto, T. *Acta Oto-Laryngol.* **1999**, *119*, 83−88.
(20) Lai, Z. F.; Imamura, T.; Koike, N.; Kitamoto, Y. *J. Biomed. Mater. Res.* **2006**, *76A*, 81−85.
(21) Rosengren, A.; Faxius, L.; Tanaka, N.; Watanabe, M.; Bjursten, L. M. *J. Biomed. Mater. Res.* **2005**, *75A*, 115−122.
(22) Garcia, Y.; Breen, A.; Burugapalli, K.; Dockery, P.; Pandit, A. *Biomaterials* **2007**, *28*, 175−186.
(23) Russ, J. C.; Dehoff, R. T., Classical stereology measures. *Practical Stereology*, 2nd ed.; Plenum Press: New York, 1999; pp 39−70.
(24) Mayhew, T. M. *Exp. Physiol.* **1991**, *76*, 639−665.
(25) Cruz-Orive, L. M.; Weibel, E. R. *Am. J. Physiol.* **1990**, *258*, L148−L156.
(26) Mandarim-De-Lacerda, C. A. *Ann. Acad. Bras. Ciênc.* **2003**, *75*, 469−486.
(27) Hahn, U.; Micheletti, A.; Pohlink, R.; Stoyan, D.; Wendrock, H. *J. Microsc.* **1999**, *195*, 113−124.
(28) Howard, C. V.; Reed, M. G. Unbiased stereology: three-dimensional measurement in microscopy. In *Advanced Methods*, 2nd ed.; Jones, C., Ed.; Garland Science/BIOS Scientific Publishers: Abingdon, Oxon, UK, 2005.
(29) Anderson, J. M. *Annu. Rev. Mater. Res.* **2001**, *31*, 81−110.
(30) Williams, D. F. *Sadhana* **2003**, *28*, 563−574.
(31) Sanders, J. E.; Lamont, S. E.; Karchin, A.; Golledge, S. L.; Ratner, B. D. *Biomaterials* **2005**, *26*, 813−818.
(32) Friedl, P.; Bröcker, E. B. *Cell Mol. Life Sci.* **2000**, *57*, 41−64.
(33) Hubbell, J. A. *Nat. Biotechnol.* **1995**, *13*, 565−576.
(34) Grinnell, F. *Trends Cell Biol.* **2003**, *13*, 264−269.
(35) Juliano, R. L.; Haskill, S. *J. Cell Biol.* **1993**, *120*, 577−585.
(36) Cukierman, E.; Pankov, R.; Yamada, K. M. *Curr. Opin. Cell Biol.* **2002**, *14*, 633−639.
(37) Buck, C. A.; Horwitz, A. F. *Annu. Rev. Cell Biol.* **1987**, *3*, 179−205.
(38) Liu, W. F.; Chen, C. S. *Mater. Today* **2005**, *8*, 28−35.
(39) Khor, E. *Biomaterials* **1997**, *18*, 95−105.
(40) Macleod, T. M.; Williams, G.; Sanders, R.; Green, C. J. *Br. J. Plastic Surg.* **2005**, *58*, 518−532.
(41) Huang-Lee, L. L.; Cheung, D. T.; Nimni, M. E. *J. Biomed. Mater. Res.* **1990**, *24*, 1185−1201.
(42) Kuribayashi, R.; Chanda, J.; Abe, T. *Artif. Organs* **1996**, *20*, 761−6.
(43) Chanda, J.; Kuribayashi, R.; Abe, T. *Ann. Thorac. Surg.* **1997**, *64*, 1063−1066.
(44) Allman, A. J.; McPherson, T. B.; Badylak, S. F.; Merrill, L. C.; Kallakury, B.; Sheehan, C.; Raeder, R. H.; Metzger, D. W. *Transplantation* **2001**, *71*, 1631−1640.
(45) Black, J. The inflammatory process. *Biological Performance of Materials: Fundamentals of Biocompatibility*, 4th ed.; Taylor & Francis: Boca Raton, FL, 2006; pp 139−164.
(46) Sampson, A. P. *Clin. Exp. Allergy* **2000**, *30*, 22−27.
(47) Bandeira-Melo, C.; Cordeiro, R. S. B.; Silva, P. M. R.; Martins, M. A. *Mem. Inst. Oswaldo. Cruz.* **1997**, *92*, 37−43.
(48) Gorczynski, R. M. *Scand. J. Immunol.* **1976**, *5*, 1031−1047.
(49) Janeway, C. A., Jr. *Immunol. Today* **1992**, *13*, 11−16.
(50) Leibovich, S. J.; Ross, R. *Am. J. Pathol.* **1976**, *84*, 501−514.
(51) Henke, C.; Marineili, W.; Jessurun, J.; Fox, J.; Harms, D.; Peterson, M.; Chiang, L.; Doran, P. *Am. J. Pathol.* **1993**, *143*, 1189−1199.
(52) Liu, H. M.; Wang, D. L.; Liu, C. Y. *Adv. Exp. Med. Biol.* **1990**, *281*, 319−331.
(53) van Tienen, T. G.; Heijkants, R. G.; Buma, P.; de Groot, J. H.; Pennings, A. J.; Veth, R. P. *Biomaterials* **2002**, *23*, 1731−1738.
(54) Manoonkitiwongsa, P. S.; Jackson-Friedman, C.; McMillan, P. J.; Schultz, R. L.; Lyden, P. D. *J. Cereb. Blood Flow Metab.* **2001**, *21*, 1223−1231.
(55) Thurston, G.; Murphy, T. J.; Baluk, P.; Lindsey, J. R.; McDonald, D. M. *Am. J. Pathol.* **1998**, *153*, 1099−1112.
(56) Hlawiczkova, M.; Gokhale, A. M.; Benes, V. *J. Microsc.* **2001**, *204*, 226−231.
(57) Dockery, P.; Perret, S.; Rogers, P. A. W.; Bulut, E. H.; Reu, B.; Warren, M. A.; Li, T.-C.; Harvey, B. J.; Jenkins, D.; Cooke, I. D. Endometrial morphology and the endometrial vascular bed. In *Disorders of the Menstrual Cycle*; O'Brien, S., Cameron, I., MacLean, A., Eds.; RCOG Press: London, 2000; p 402.

BM700560K